Spatial prediction of the runoff coefficient in Southern Peninsular Italy for the index flood estimation

G. Del Giudice, R. Padulano and G. Rasulo

ABSTRACT

The runoff coefficient φ is a crucial parameter for the estimation of the mean value of annual maximum flood peak discharges in ungauged watersheds, where no direct measures are available. If the rational method is applied as a rainfall–runoff transformation model, the runoff coefficient accounts for all the hydrological losses, and it can be conceptually defined as the fraction of the total rainfall contributing to the flood peak response. In the present paper, focusing on Southern Peninsular Italy, a regression model is proposed to improve the prediction of the above defined runoff coefficient as a function of several parameters describing both morphological and mean annual climatic watershed characteristics. Morphological features are described by using the Soil Conservation Service permeability classification and the related variable S, referred to an average antecedent moisture condition. Different climatic indices enable a subsequent enhancement of S in order to account for the specific mean annual moisture condition of each watershed.

Key words | climatic factor, index flood, maximum potential retention, rainfall–runoff models, rational method, runoff coefficient

G. Del Giudice
R. Padulano (corresponding author)
G. Rasulo
Department of Civil, Architectural and Environmental Engineering,
Federico II University,
Naples,
Italy
E-mail: *roberta.padulano@unina.it*

INTRODUCTION

The estimation of the probability distribution of annual maximum flood peak discharges is a key factor in engineering practice. Nevertheless, whereas flood frequency can be directly assessed within gauged watersheds, where direct measures are available, its evaluation is not straightforward for ungauged watersheds, where other considerations must be held. Generally, a regional analysis is undertaken so that some homogeneous regions, within which the probability distribution of annual maximum flood peak discharges can be considered invariant, can be determined. The criteria which allow the definition of homogeneous regions are known as 'hydrological similitude criteria' (Penta *et al.* 1972; Rossi *et al.* 1984; Cunnane 1988; Hosking & Wallis 1997). In each homogeneous region, some statistical parameters are assumed as a constant, so that in any watershed the probability distribution of peak discharges is known once a scale parameter, depending on the specific watershed characteristics, is defined. One of the most common regional flood frequency analysis methods is the index flood method (Dalrymple 1960; Riggs 1973), in accordance with which the annual maximum flood peak discharge Q_T, with return period T, can be estimated as the product of a dimensionless growth factor K_T, depending on the return period T and invariant in each homogeneous region, and a scale parameter μ_Q known as the index flood, depending on the investigated watershed features.

In gauged watersheds, a direct analysis of discharge data leads to the estimation of the index flood, which is generally assumed coincident with the mean of annual maximum flood peaks, whereas a few flood estimation procedures adopt the median (IH 1999; Preti *et al.* 2011). In ungauged watersheds, the literature provides few methods which relate the index flood to different parameters describing watershed features (Brath *et al.* 2001; Kjeldsen & Jones 2010), such as morphology, land use, and climate. One of the most commonly adopted methods for the estimation of the index flood is the rational method (Mulvaney 1851; Turazza 1880; Smith & Lee 1984; Moisello 1999; Brath

doi: 10.2166/nh.2013.243

et al. 2001); in accordance with the model, the mean of annual maximum flood peak discharges is directly related to the mean of annual maximum peak rainfall intensity over the basin, for a duration equal to the watershed time of concentration (defined as the time taken by a droplet falling on the most remote point of a drainage basin to reach the outlet), through a parameter known as runoff coefficient φ. Because the latter captures the fraction of 'quick flow' runoff to the event precipitation, it is defined throughout the paper as 'flood' runoff coefficient to differentiate it from the annual runoff coefficient which is the fraction of total annual runoff (including 'low flow') to annual precipitation. The so estimated flood runoff coefficients conceptually describe both the fraction of rainfall volume retained by the soil and the vegetation (i.e., the transformation of the total rainfall in net rainfall as a result of processes such as infiltration, canopy interception, and surface detention), and the dampening effect of the catchment, which implies the reduction of the flood peak as compared to the net rainfall intensity (Preti et al. 2011). Generally, this coefficient can be estimated thanks to correlations with some watershed descriptors, which typically only account for lithology, whereas the influence of land use is often neglected (Iacobellis & Fiorentino 2000; Brath et al. 2001).

Nowadays, many studies exist which investigate both the spatial and temporal variability of the runoff coefficients (Naef 1993; Gottschalk & Weingartner 1998; Wainwright & Parson 2002; Cerdan et al. 2004; Scherrer et al. 2007; Viglione et al. 2009; Merz & Blöschl 2009). Typically, these studies focus on an event runoff coefficient which is a key parameter in the application of lumped conceptual rainfall–runoff transformation models, referring to generic event durations, different from the time of concentration (Viglione et al. 2009). Since both the event runoff coefficient and the flood runoff coefficient, coupled with the rational method, describe the same physical phenomenon, accounting for all types of hydrological losses, the same considerations can be held, at least as regards spatial variability. Some existing studies have indeed tried to relate the runoff coefficient to several indicators describing both morphological and climatic watershed features, investigating both small and large watersheds, with very different results. Scherrer et al. (2007), analyzing a group of hillslopes in Switzerland, observed a great variability in the runoff coefficient values, concluding that the partition process operated by the runoff coefficient, though related to physical features such as vegetation, slope, soil clay content, and others, cannot always be directly linked to the parameters usually adopted to represent them. Cerdan et al. (2004), in France, observed a significant decrease in the runoff coefficient with increasing watershed extent, and its relevant dependence on the percentage of arable land for extents of about 10 km^2; a similar influence of areas was observed by Wainwright & Parson (2002). Gottschalk & Weingartner (1998) analyzed 17 Swiss watersheds and found that the differences in runoff coefficients could be partially explained by topographic and geomorphologic characteristics, such as altitude, slope, stream network density, and geology. A large event analysis in Austria was undertaken by Merz & Blöschl (2009), who found that the main controls on the runoff coefficient were the climate and the runoff regime through the seasonal catchment water balance, while other parameters, such as geology and land use, had a poor influence. A totally different approach is that of Naef (1993), who analyzed about 100 Swiss watersheds and concluded that the interaction between runoff coefficient and catchment features is so complex that runoff coefficients should be treated as a random variable.

The aim of this paper is to investigate the spatial variability of the flood runoff coefficient at a regional scale, by analyzing 50 watersheds placed in Southern Peninsular Italy. A multivariate regression model is proposed to improve the prediction of the runoff coefficients as a function of several parameters describing both morphological and mean annual climatic watershed characteristics; this choice was made because long-term controls, such as climate, do not vary at a short time scale and hence may contribute only to the spatial variability of runoff coefficients (Merz & Blöschl 2009). The so predicted flood runoff coefficients enable the estimation of the mean value of the annual maximum flood peak discharges in ungauged river sections, by using the rational method.

MOTIVATION AND GENERAL APPROACH

The application of most of the cited studies about the runoff coefficient require information not easily available for

analyses whose aim is to predict the flood runoff coefficient in a generic ungauged watershed, especially those concerning advanced climatic data (i.e., solar radiation, that could be useful in order to compute evapotranspiration with a physical-based model, such as Penman (1948), Monteith (1965), Priestley & Taylor (1972), and Hargreaves & Samni (1982)). In this paper, such an analysis is performed with simple parameters and relations, commonly adopted in engineering practice, which only require open source data, easily available.

In particular, the Hydrogeological Map of Southern Italy (Allocca *et al.* 2007) is adopted to represent outcropping geological formations of the investigated watersheds, properly modified by inserting a pyroclastic rock cover within some areas of Campania Region (Rasulo *et al.* 2009). In addition, land use/covers are derived from the Corine (COoRdination of INformation on Environment) Land Cover digital maps (Bossard *et al.* 2000) with reference to satellite images of 2000. Climatology is represented by using rainfall and temperature data available on the SCIA system web site (National system for the collection, processing and diffusion of climatic data of environmental interest – http://www.scia.sinanet.apat.it), which provides mean annual and monthly precipitation and temperature data measured in 1629 and 144 stations, respectively, covering the period 1961–1990. Those at-site data can be processed so as to have mean annual and monthly precipitation and mean annual and monthly temperature maps, respectively.

Whereas both climatic and land use/cover data cover the whole Italian surface, the Hydrogeological Map is limited to Southern Italy, and in particular to the regions of Campania, Puglia, Basilicata, and Calabria (Figure 1). The adoption of a different mapping for the hydrogeological information would have collided with the need of handling homogeneous information; thus, it seemed more coherent to limit the extent of our analysis to the 50 gauged watersheds in Southern Peninsular Italy.

Hydrometric data have already been processed by the Operative Units of the National Group for the Prevention from Hydrogeological Disasters (GNDCI), within the special project on 'Flood Evaluation' (VAPI) supported by the National Research Council (CNR) of Italy. They can be found in the regional VAPI reports (Versace *et al.* 1989; Claps *et al.* 1994; Rossi & Villani 1994).

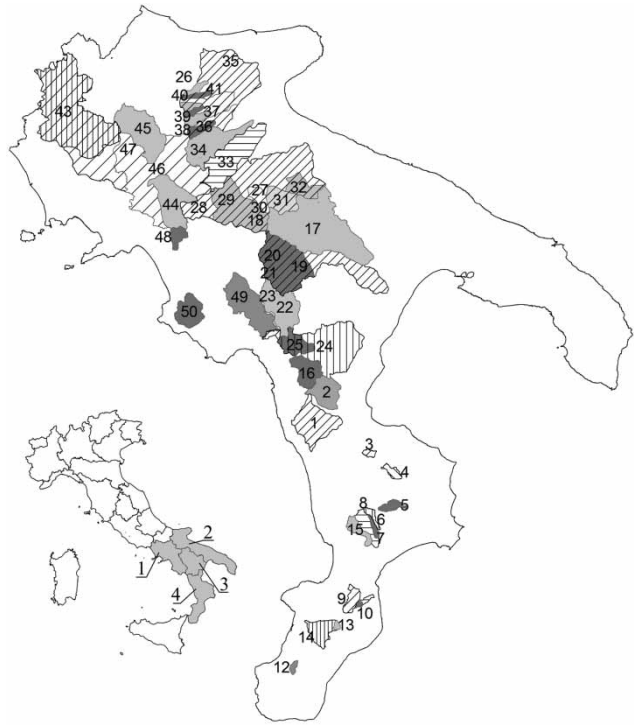

Figure 1 | In the Italian Peninsula view the investigated areas are highlighted: Campania (1), Puglia (2), Basilicata (3), and Calabria (4). In the Southern Italy view the investigated watersheds are numbered (see Table 1 for watershed names and features).

DATA

In the present study, 50 gauged river basins within Southern Italy are analyzed, with areas ranging between 15 and 5,500 km^2. Table 1 shows a set of hydrological and geomorphological parameters, such as the mean values of annual maximum flood peak discharges μ_Q, in [m^3 s^{-1}] (computed as an arithmetical mean over the available recorded years), and morphological parameters, such as basin extent A, in [km^2], main channel length L, in [km], mean watershed elevation h_m, in [m a.s.l.], river slope i, in [%] and time of concentration t_C, in [h], in accordance with Giandotti's formula (Giandotti 1934) which is still widely used in hydrological practice in Italy.

The total number of available gauged river sections VAPI reports provide (Versace *et al.* 1989; Claps *et al.* 1994; Rossi & Villani 1994) is slightly more than 50; indeed, some drainage basins were dropped since they

Table 1 | Watershed data

id	Watershed	μ_Q ($m^3 s^{-1}$)	A (km^2)	L (km)	h_m (m a.s.l.)	i (%)	t_c (h)	R (mm)	D (mm)
1	Esaro a La Musica	328.84	532.68	37.64	496	1.24	8.80	1,469	663
2	Coscile a Camerata	80.37	303.54	26.66	725	2.68	5.31	1,206	640
3	Trionto a Difesa	8.74	31.73	8.95	1,118	0.97	3.87	1,172	584
4	Lese a Schiena D'Asino	18.99	60.67	21.23	1,120	2.94	3.78	1,365	752
5	Tacina a Rivioto	81.19	77.56	23.33	1,332	3.55	2.73	1,360	940
6	Alli a Orso	16.70	45.48	19.61	1,076	2.59	2.82	1,089	874
7	Melito a Olivella	17.20	41.26	17.28	863	3.28	2.90	1,277	618
8	Corace a Grascio	151.66	177.63	35	820	1.82	4.87	1,399	683
9	Ancinale a Razzona	82.37	116.02	24.23	880	1.14	5.19	1,703	1,022
10	Alaco a Mammone	13.63	14.85	3.87	1,051	1.31	2.86	1,820	1,199
11	Alaco a Pirrella	15.62	38.02	14.23	893	2.66	2.25	1,748	1,124
12	Duverso a S. Giorgìa	12.88	28.69	10.5	971	8.59	1.88	1,777	949
13	Metramo a Castagnara	6.39	19.77	4.52	1,007	3.54	2.13	1,763	1,526
14	Metramo a Carmine	73.08	233.08	26.93	516	1.66	5.75	1,521	631
15	Amato a Marino	79.23	114.69	31.78	758	1.69	4.58	1,422	677
16	Lao a Piè di Borgo	211.20	279.99	20.27	832	1.76	5.13	1,515	967
17	Bradano a San Giuliano	539.15	1,657.60	100.83	440	0.38	20.38	685	133
18	Bradano a Ponte Colonna	184.08	461.62	52.96	560	0.62	11.13	689	136
19	Basento a Menzena	405.63	1,402.84	127.11	664	0.53	16.77	796	274
20	Basento a Gallipoli	359.84	859.86	51.48	893	1.01	10.95	875	338
21	Basento a Pignola	36.87	43.66	12.53	1,074	3.70	3.10	1,010	568
22	Agri a Tarangelo	188.68	510.66	37.56	870	0.81	9.17	1,095	619
23	Agri a Le Tempe	84.50	173.67	18.37	933	1.47	5.38	1,099	803
24	Sinni a Valsinni	497.14	1,141.08	69.31	752	0.93	12.18	1,151	566
25	Sinni a Pizzutello	234.24	232.73	32.23	932	1.58	6.20	1,572	988
26	Canale S. Maria	17.95	58.11	17.71	201	1.26	6.77	650	90
27	Ofanto a S. Samuele di Cafiero	517.60	2,716.33	142.13	454	0.29	25.65	725	155
28	Ofanto a Cairano	208.02	266.46	32.23	674	0.74	8.29	974	341
29	Ofanto a M.te Verde Scalo	516.63	1,017.46	55.96	657	1.04	13.44	867	250
30	Arcidiaconata a P.Rapolla.-Lavello	45.08	123.96	18.77	530	2.98	3.96	756	175
31	Venosa a Ponte S. Angelo	61.87	263.73	39.34	502	0.81	8.90	666	157
32	Locone a Ponte Brandi	40.25	219.75	22	340	1.02	8.11	659	53
33	Carapelle a Carapelle	277.42	714.86	76.58	510	0.27	12.92	613	128
34	Cervaro ad Incoronata	217.27	540.23	78.49	379	0.74	14.53	676	128
35	Candelaro a Str. Bonifica N. 24	158.14	1,778.14	60.48	240	0.28	21.37	599	51
36	Celone a a S. Vincenzo	34.19	92.59	23.82	532	2.11	5.01	724	178
37	Celone a Ponte Foggia S. Severo	43.25	237.00	43.82	380	1.10	8.90	626	95
38	Vulgano a Ponte Troia-Lucera	72.86	94.37	22.24	486	2.06	5.08	729	117
39	Salsola a Casanova	45.06	44.13	16.55	444	2.60	3.99	673	107
40	Casanova a Ponte Lucera-Motta	25.71	57.38	15.22	474	2.19	3.86	692	112

(*continued*)

Table 1 | continued

id	Watershed	μ_Q ($m^3 s^{-1}$)	A (km^2)	L (km)	h_m (m a.s.l.)	i (%)	t_c (h)	R (mm)	D (mm)
41	Salsola a Ponte Foggia-S.Severo	74.49	455.73	47.24	235	0.85	13.97	635	86
42	Triolo a Ponte Lucera-Torremaggiore	38.48	55.97	21.95	302	1.44	5.66	649	110
43	Volturno ad Amorosi	636.28	1,950.14	114.1	540	0.37	19.35	1,353	486
44	Calore Irpino ad Apice	325.01	547.99	48.5	607	1.05	9.76	1,121	706
45	Tammaro a Paduli	213.49	660.28	69.2	597	0.66	11.88	1,010	368
46	Calore Irpino a Solopaca	995.05	2,967.78	106.2	536	0.38	21.32	1,107	407
47	Volturno a Ponte Annibale	1,296.75	5,493.42	146.3	534	0.26	28.38	1,183	538
48	Tusciano ad Olevano sul Tusciano	40.37	104.13	19.5	940	4.46	3.08	1,633	1,195
49	Tanagro a Polla	213.10	627.55	56.9	812	0.52	11.88	1,273	489
50	Alento a Casalvelino	261.36	285.67	28.3	350	0.71	7.41	1,240	481

Note: mean of maximum annual peak flood (index flood) μ_Q; basin area A; length of the longest watercourse to the basin outlet L; mean basin altitude h_m (meters above sea level); average watershed slope i; time of concentration computed using the Giandotti equation t_c; mean annual values of rainfall (R) and runoff (D) provided by the Italian Hydrologic Yearbooks (SIMN, Annali Idrologici).

presented an anomalous unit discharge [$m^3 s^{-1} km^2$] if compared to the watersheds belonging to the same river but situated upstream or downstream, and this could be evidence of errors in discharge data. Furthermore, drainage basins with dam or diversion structures were not considered.

Histograms in Figure 2 show the frequency distribution of hydromorphological features within the investigated watersheds grouping each feature into mutually exclusive 10 classes. A large number of watersheds have an area smaller than 550 km^2, a main river length lower than 45 km, and a river slope lower than 2%.

The time of concentration t_C has a frequency distribution with a shape similar to that of the river length, whereas the distribution of μ_Q resembles that of the areas. A and L distributions show a large skewness, while h_m has a more uniform profile.

Table 1 also shows the mean annual values of rainfall (R) and runoff (D), provided by the Italian Hydrologic Yearbooks (SIMN, Annali Idrologici) for the gauged river sections, whereas Table 2 shows a basin-averaged mean annual precipitation value (P) and a similar basin-scale average for the mean annual temperature (τ), both values derived from the SCIA maps above defined.

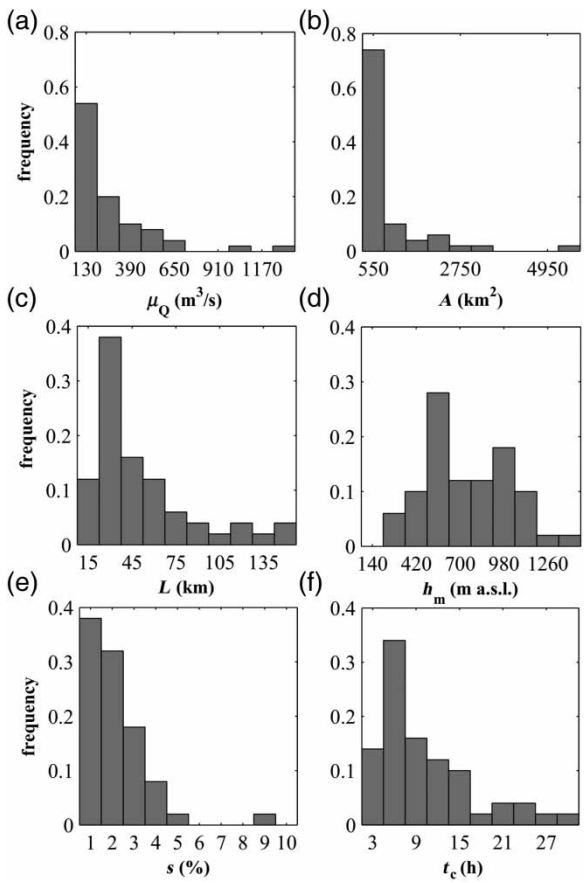

Figure 2 | Morphological features of investigated watersheds.

Table 2 | Watershed indicators

id	φ_o	S (mm)	ET (mm)	P (mm)	τ (°C)	ET_P (mm)	ϕ	LF (mm/°C)
1	0.442	129	806	1,171	13.04	731	0.62	89.82
2	0.117	158	565	1,161	13.21	741	0.64	87.87
3	0.064	132	588	1,061	12.72	713	0.67	83.47
4	0.077	167	614	1,144	12.94	724	0.63	88.37
5	0.190	175	420	1,199	13.28	739	0.62	90.30
6	0.068	167	215	1,283	13.11	733	0.57	97.91
7	0.083	168	658	1,228	13.22	737	0.60	92.86
8	0.274	161	716	1,241	13.18	735	0.59	94.20
9	0.155	159	681	1,318	13.51	741	0.56	97.59
10	0.125	191	621	1,356	13.49	741	0.55	100.47
11	0.055	180	624	1,326	13.48	741	0.56	98.36
12	0.066	146	828	1,108	15.54	814	0.74	71.30
13	0.050	177	237	1,316	13.89	753	0.57	94.78
14	0.116	150	890	1,184	14.32	768	0.65	82.74
15	0.228	150	745	1,211	13.19	734	0.61	91.77
16	0.325	157	548	1,291	13.27	741	0.57	97.29
17	0.438	72	552	655	13.57	752	1.15	48.33
18	0.364	72	553	693	13.28	742	1.07	52.17
19	0.334	86	522	731	13.58	752	1.03	53.88
20	0.380	86	537	780	13.36	743	0.95	58.37
21	0.316	117	442	843	13.35	743	0.88	63.18
22	0.254	136	476	1,152	13.28	739	0.64	86.79
23	0.248	157	296	1,136	13.34	742	0.65	85.17
24	0.300	99	585	1,031	13.33	743	0.72	77.38
25	0.538	115	583	1,340	13.16	735	0.55	101.80
26	0.217	89	561	699	13.53	754	1.08	51.63
27	0.441	99	569	726	13.15	737	1.01	55.29
28	0.665	105	634	1,013	13.18	734	0.72	76.87
29	0.628	99	617	876	13.06	732	0.84	67.05
30	0.166	103	580	715	13.03	732	1.02	54.88
31	0.210	88	509	667	13.14	737	1.10	50.80
32	0.149	108	606	613	13.37	746	1.22	45.83
33	0.506	81	485	668	13.06	734	1.10	51.22
34	0.543	94	549	723	13.17	738	1.02	54.92
35	0.191	106	547	674	13.52	753	1.12	49.88
36	0.177	95	546	773	13.32	744	0.96	58.04
37	0.161	94	530	720	13.33	746	1.04	54.01
38	0.382	93	612	781	13.36	746	0.95	58.50
39	0.433	97	566	773	13.39	747	0.97	57.75
40	0.189	94	580	759	13.41	749	0.99	56.65

(*continued*)

Table 2 | continued

id	φ_o	S (mm)	ET (mm)	P (mm)	τ (°C)	ET_P (mm)	ϕ	LF (mm/°C)
41	0.234	94	550	712	13.43	750	1.05	53.07
42	0.412	90	539	703	13.50	752	1.07	52.05
43	0.452	173	867	1,277	14.17	770	0.60	90.10
44	0.496	129	415	1,057	13.47	745	0.70	78.41
45	0.378	87	642	971	13.53	748	0.77	71.76
46	0.623	106	700	989	13.52	747	0.76	73.10
47	0.466	133	645	1,108	13.83	758	0.68	80.05
48	0.080	239	438	1,209	13.84	758	0.63	87.36
49	0.296	191	784	1,312	13.52	748	0.57	97.02
50	0.583	104	759	1,203	14.18	770	0.64	84.85

Note: observed flood runoff coefficient φ_o; maximum potential retention S; actual evapotranspiration ET (=R–D); mean annual precipitation P from SCIA maps; mean annual temperature P from SCIA maps; mean annual potential evapotranspiration ET_p; Budyko Index ϕ; Lang Pluviofactor LF.

METHODOLOGY

In the following, the three main steps of the analysis will be described. In the first step, flood runoff coefficients will be evaluated for the 50 gauged river sections, as those values that enable the estimation of mean annual flood peak discharges in Table 1. In the second step, indicators of geologic, land use, and climatic controls will be defined. In the third step, a model that enables the estimation of a correlation between the flood runoff coefficient and the chosen indicators will be described.

Observed runoff coefficient

For each of the available 50 gauged watersheds, the flood runoff coefficient can be easily estimated by applying a lumped conceptual rainfall–runoff transformation model; the previously mentioned rational method provides:

$$\mu_Q = \frac{\varphi \cdot \mu[I_A(A, d, T)] \cdot A}{3.6} \tag{1}$$

where (i) μ_Q is the mean annual flood peak discharge (index flood), in [$m^3 s^{-1}$]; (ii) φ is the flood runoff coefficient assumed to be independent of rainfall duration and intensity; (iii) $\mu[I_A(A, d)]$ is the mean of annual maximum rainfall intensity over the basin, in [mm h^{-1}], whose duration d is equal to the concentration time t_C of the watershed; (iv) A is the watershed area, in [km^2].

$I_A(A, d, T)$ can be defined as follows:

$$I_A(A, d, T) = ARF(A, d, T) \cdot I_P(d, T) \tag{2}$$

where ARF is the areal reduction factor. Only a few empirical relations are available to compute ARF; the Eagleson formula was adopted (Eagleson 1972), with the dimensional coefficients C_1, C_2, and C_3 calibrated for Southern Peninsular Italy basins (Versace *et al.* 1989; Claps *et al.* 1994; Rossi & Villani 1994):

$$ARF(A, d) = 1 - \left(1 - e^{-C_1 A}\right) \cdot e^{-C_2 d^{C_3}} \tag{3}$$

Equation (3) does not depend on the return period, whose effect is still negligible in the investigated basins (Rossi & Villani 1994).

Once the ARF values have been computed for each watershed, the estimation of intensity-duration-frequency (IDF) curves, representing the maximum point rainfall intensity $I_P(d, T)$ as a function of duration d and return period T (Koutsoyiannis & Manetas 1998), is required to compute $I_A(A, d)$. In the present paper, the IDF curves provided by the VAPI project for each region were adopted.

In order to estimate the time of concentration t_C, the Giandotti formula (Equation (4)) (Giandotti 1934) was adopted:

$$t_C = \frac{4\sqrt{A} + 1.5L}{0.8\sqrt{h_m - h_0}} \tag{4}$$

where (i) t_C is the watershed time of concentration, in [h]; (ii) A is the drainage basin area, in [km^2]; (iii) L is the length of the longest watercourse to the drainage basin outlet, in [km]; (iv) h_m is the mean drainage basin elevation, in [m a.s.l.]; (v) h_0 is the drainage basin outlet elevation, in [m a.s.l.]. The Giandotti formula is one of the relations calibrated for a wide range of watershed extents (between 170 and 70,000 km^2) so it is appropriate for larger basins (Miliani *et al.* 2011), and it is the most commonly used in Italy when adopting indirect methods for the estimate of the index flood (Brath *et al.* 2001; Rasulo *et al.* 2009, Preti *et al.* 2011).

Finally, the 'observed flood runoff coefficient' φ_o for each gauged river section can be computed by inverting Equation (1) (Rasulo *et al.* 2009; Preti *et al.* 2011) and considering $d = t_C$ (Brath *et al.* 2001):

$$\varphi_o = \frac{\mu_Q}{ARF(A, t_C) \cdot \mu[I_P(t_C)] \cdot A} \tag{5}$$

where $\mu[I_P(t_C)]$ is the mean value of IDF curve for maximum point rainfall.

Although the obtained φ_o data contain uncertainties, due to the approximations in the evaluation of both ARF and I_P, they were assumed to be the most precise estimations that could be obtained with the available data.

Definition of indicators

Geology and land use controls

Soil permeability depends on a combined effect of surface geology and land use; their control on the runoff coefficient is theoretically very strict, since runoff coefficients are expected to increase as permeability decreases. Thus, a simple and widely used classification of soil permeability was adopted, that could account for both geology and land use with a single variable; that classification is the one proposed by the Soil Conservation Service (SCS 1972). According to the SCS, a single parameter, namely the curve number (CN), can be used to describe soil permeability, ranging between 0, meaning a highly permeable soil, and 100, meaning a totally impervious surface. Alternatively, a different parameter can be used, that is the maximum potential retention S, in [mm], which is related to CN by Equation (6):

$$S = 254\left(\frac{100}{\mathrm{CN}} - 1\right) \tag{6}$$

Unlike CN, S has some different physical interpretations (van Dijk 2010); the SCS one was chosen (SCS 1972), which explains S as the maximum water level each soil can retain in accordance with its characteristics. SCS classifies soils into four hydrological soil groups (HSG), A, B, C, D, with a decreasing permeability level from A to D (SCS 1972). For each HSG, S values can vary depending on land uses, land treatments, hydrological conditions, and antecedent moisture conditions (AMC), the latter corresponding to the rainfall depth in the 5 days preceding each flood event (Mishra *et al.* 1999; Beven 2001; Sahu *et al.* 2010; Wang *et al.* 2012).

In order to obtain a similar classification for Italian soils, the four levels of hydrogeological units permeability proposed by the Hydrogeological Map (Allocca *et al.* 2007) were assumed corresponding to the SCS HSG (A = high, B = moderate, C = low, D = very low infiltration rates), so that each Southern Italian hydrogeological unit could be assigned to a HSG (Table 3).

Subsequently, Corine land use/covers were cross-combined with the SCS land uses by associating the ones with similar characteristics (Table 4). To carry out the matching operation, some already studied correspondences between SCS and Corine land use/cover were taken into account (Mancini & Rosso 1989; Miliani *et al.* 2011). When S was found to vary, for the same land use, among all the possible different land treatments and hydrological conditions, the mean value was considered; this was performed because land treatments are more variable in time than land use practices, whereas hydrological conditions cannot be known on such a large scale. Furthermore, since the purpose of the procedure is not to identify the soil permeability during a particular rainfall event, but only to grade the relative soil permeability as a partial indicator of the mean response of the watershed, the S values corresponding to the normal (average) AMC condition were adopted. Table 4 provides the S values, in [mm], as a classification of the different soil permeability for each hydrologic soil group and land use.

Table 3 | Correspondence between hydrogeological units and HSG

Hydrogeological units	Unit permeability (HSG)
Alluvial-coastal	B
Lake	C
Continental epiclastic sediments	B
Travertine	A
Calabrian 'Alteriti'	B
Pyroclastic-fall deposits	B
Pyroclastic-flow deposits	B
Lava	A
Sand-conglomerate	B
Clay	D
Molassic sediments	B
Messina evaporites	B
Sandstone-conglomerate	B
Sandstone-limestone-pelite succession	C
Limestone-pelite succession	C
Transitional calcarenite-marl	B
Apulia platform limestone	A
Limestone from Mount Marzano Unit and Maddalena Mountains unit	A
Dolomite from Maddalena Mountains and Mount Foraporta unit	B
Limestone from Alburno-Cervati-Pollino unit	A
Dolomite from Alburno-Cervati Pollino unit	B
Dolomite from Bulgheria-Verbicaro unit	B
Limestone from San Donato unit metamorphic	B
Silicate-marl from Lagonegro unit I and II	C
Limestone with flint from Lagonegro unit I and II	B
Marl-sandstone-pelites from Molise unit	C
Limestone-Marl from Molise Unit	B
Metapelite-metacalcareous Frido unit	C
Ophiolite from Frido unit	C
Limestone-clay from North-Calabrian unit	B
Clay-limestone from Sicilian unit	D
Igneous rocks	B
Metamorphic rocks	C
Fractured metamorphic rocks	B
Limestone	C
Surface water	D
Limestone from Matese-Mount Maggiore and Monte Alpi unit	A
Lim. with pyroclastic cover from Matese-Mount Maggiore and Monte Alpi unit	B
Dolomite from Matese-Mount Maggiore and Monte Alpi unit	B
Dolomite with pyroclastic cover from Matese-Mount Maggiore and Monte Alpi unit	C
Limestone from Picentino-Taburno unit	A
Limestone with pyroclastic cover from Picentino-Taburno unit	B
Dolomite-marl from Picentino-Taburno unit	B
Dolomite-marl with pyroclastic cover from Picentino-Taburno unit	C
Limestone from Bulgheria-Verbicaro unit	A
Limestone with pyroclastic cover from Bulgheria-Verbicaro unit	B

Two caveats must be mentioned. The first regards the reliability of the SCS-CN method, which is by now a highly debated issue; it should be highlighted that such a method has not been applied for the prediction of the runoff coefficient, but only the soil classification has been used (Merz *et al.* 2006).

The second observation concerns the Corine map. Indeed, that map was assumed to be representative of the whole period in which the annual peak flood data were collected in the gauged river sections of the drainage basins shown in Table 1. However, this assumption is not restrictive because (i) the effect of urbanization and therefore the increase in impervious surfaces do not affect soil permeability, given their limited extension with respect to natural basins (Ranzi *et al.* 2002), and (ii) the massive reforestation works which occurred during the last postwar period have caused a change in land use from 'pastures' to 'woods', with an overall negligible increase in the values of potential maximum retention S.

Climatic controls

Along with geology and land use, climate also influences soil permeability; indeed, it indirectly impacts upon the

Table 4 | Maximum potential retention *S* (mm)

id	CORINE code	CORINE land cover	SCS land use	S (mm) according to HSG A	B	C	D
1	1.1.1	Continuous urban fabric	Urban districts I.A. 85%	31	22	16	13
2	1.1.2	Discontinuous urban fabric	Urban districts I.A. 65%	76	45	28	22
3	1.2.1	Industrial or commercial units	Industrial districts	60	35	25	19
4	1.2.2	Road and rail networks and associated land	Paved streets and roads; curbs and storm drains	5	5	5	5
5	1.2.4	Airports	Urban districts I.A. 65%	76	45	28	22
6	1.3.1	Mineral extraction sites	Open space g.c. <50%	114	64	38	19
7	1.3.2	Dump sites	Open space g.c. <50%	114	64	38	19
8	1.3.3	Construction sites	Open space g.c. < 50%	76	41	25	16
9	1.4.1	Green urban areas	Open space g.c. >75%	397	162	89	64
10	1.4.2	Sport and leisure facilities	Open space g.c. 50–75%	264	114	68	48
11	2.1.1	Non-irrigated arable land	Small grain	156	94	60	45
12	2.1.2	Permanently irrigated land	Close-seeded legumes or rotational meadows	169	99	60	48
13	2.2.1	Vineyards	Row crops	125	80	52	41
14	2.2.2	Fruit trees and berry plantations	Woods–grass combination	323	137	76	56
15	2.2.3	Olive groves	Woods–grass combination	323	137	76	56
16	2.3.1	Pastures	Meadow (good H.C.)	381	156	89	45
17	2.4.1	Annual crops associated with permanent crops	Woods–grass combination (poor H.C.)	192	94	56	41
18	2.4.2	Complex cultivation patterns	Close-seeded legumes or rotational meadows	169	99	60	48
19	2.4.3	Land principally occupied by agriculture, with significant areas of natural vegetation	Woods–grass combination	323	137	76	56
20	2.4.4	Agro-forestry areas	Woods–grass combination	323	137	76	56
21	3.1.1	Broad-leaved forest	Woods	432	169	94	64
22	3.1.2	Coniferous forest	Woods	432	169	94	64
23	3.1.3	Mixed forest	Brush-brush-weed-grass mixture	493	275	192	149
24	3.2.1	Natural grasslands	Meadow v.c. <50%	120	68	41	31
25	3.2.2	Moors and heathlands	Pinyon, juniper, or both with grass understorey	323	184	94	64
26	3.2.3	Sclerophyllous vegetation	Sagebrush with grass understorey	397	244	149	109
27	3.2.4	Transitional woodland-shrub	Sagebrush with grass understorey (H.C. fair)	452	244	149	109
28	3.3.1	Beach, dunes, sand	Saltbush, greasewood, creosote-bush, bursage, blackbrush, palo verde, mesquite, and cactus	200	99	56	41
29	3.3.2	Bare rocks	Saltbush, greasewood, creosote-bush, bursage, blackbrush, palo verde, mesquite, and cactus	200	99	56	41
30	3.3.3	Sparsely vegetated areas	Saltbush, greasewood, creosote-bush, bursage, blackbrush, palo verde, mesquite, and cactus	200	99	56	41
31	3.3.4	Burnt areas	Saltbush, greasewood, creosote-bush, bursage, blackbrush, palo verde, mesquite, and cactus	200	99	56	41

mechanisms of flood generation through the seasonality of rainfall and evapotranspiration, which thus affect the AMC of a watershed for each single storm event (Sivapalan *et al*. 2005). The above-mentioned *S* values do not account for this effect because they correspond to a homogeneous antecedent moisture condition (AMC II) for all soils of the basins. However, SCS provides *S* values for different antecedent soil moisture conditions, higher for dry soils, lower for

moist soils. Thus a suitable improvement of flood runoff coefficient estimate could be achieved correcting S values by using an appropriate antecedent soil moisture condition. To describe the mean annual antecedent moisture condition, the above-mentioned precipitation and temperature data are used, combined in different indices which will be generically referred to as climatic indices (*CI*).

Based on the available climatic data, the chosen indices are the mean annual precipitation P, the Budyko Index ϕ, the Lang Pluviofactor *LF*.

The Budyko Index (Budyko 1974) is an aridity index defined as the ratio of annual potential evapotranspiration ET_p, in [mm], to annual precipitation P, in [mm]:

$$\phi = ET_p/P \tag{7}$$

Regions where aridity index is greater than unity are broadly classified as dry since the evaporative demand cannot be met by precipitation; similarly, regions with a less than unity index are classified as wet. Under some simplifying assumptions (Arora 2002), the Budyko Index is usually related to the ratio of actual evapotranspiration ET to precipitation; many functional forms exist (Schreiber 1904; Ol'dekop 1911; Turc 1954; Pike 1964) that describe this relation. Actual evapotranspiration ET was evaluated, under the same simplifying assumptions (Arora 2002), as a difference between rainfall R and runoff D measured in the investigated gauged river sections. Then the evaporation ratio is computed as ET/R. As regards the estimate of annual ET_p, only the empirical method of Thornthwaite (1948) can be applied to the data collected for this study, since it only accounts for monthly temperatures.

Lang Pluviofactor (Lang 1915) is defined as the ratio of mean annual precipitation to mean annual temperature:

$$LF = P/\tau \tag{8}$$

where P is the mean annual precipitation over a watershed, in [mm], and τ is the mean annual temperature, in [°C]. *LF* was computed by using, for P and τ, the values derived from the SCIA maps.

Table 2 provides the basin-averaged values of the above-mentioned *CI*.

Computational method

The prediction of the flood runoff coefficient is achieved by computing, for each gauged watershed, an 'estimated flood runoff coefficient' φ_e which minimizes an objective function of error, namely the square sum of errors *SSE*:

$$SSE = \sum_{i=1}^{N} (\varphi_{o,i} - \varphi_{e,i})^2 \tag{9}$$

where N is the number of gauged basins, whereas $\varphi_{o,i}$ and $\varphi_{e,i}$ are, respectively, the basin-averaged observed and estimated runoff coefficients for the watershed i.

The basin-averaged estimated flood runoff coefficient is defined as follows:

$$\varphi_{e,i} = \frac{\sum_{j=1}^{J} \varphi_{e,j} \cdot A_j}{A_i} \tag{10}$$

where $\varphi_{e,j}$ is the estimated runoff coefficient value for every elementary area A_j, characterized by a specific combination of outcropping geological formations and land use, and J is the total number of elementary areas within each watershed A_i.

Once the objective function was defined, the existence of a correlation between the flood runoff coefficient and the geology–land use combinations, numerically expressed by the variable S, was investigated; the chosen relation between the two parameters is the following:

$$\varphi_{e,j} = \min\lfloor e^{\alpha S_j + \gamma}, 1 \rfloor \tag{11}$$

where S_j is the maximum potential retention value of each elementary area, whereas α, in [mm^{-1}], and γ, dimensionless, are the fitting parameters. A linear relationship was considered at first, but was rejected since it provides meaningless values such as $\varphi > 1$ and $\varphi < 0$ for extreme S values. The exponential Equation (11) causes $\varphi = 0$ for $S \to \infty$, but $\varphi > 1$ for $S \to 0$; when φ was found to be greater than 1, it was manually set as equal to 1.

Subsequently, it was investigated whether the introduction of climatic information, expressed by the variable *CI*

(i.e., the mean annual precipitation P, the Budyko Index ϕ, or the Lang Pluviofactor LF), significantly improved the prediction of runoff coefficients. Estimated flood runoff coefficient for each elementary area was expressed as follows:

$$\varphi_{e,j} = \min\left[e^{\alpha S'_j + \gamma}, 1\right] \tag{12}$$

where S'_j is the new S value of every elementary area j, corrected by means of its climatic index:

$$S'_j = S_j \cdot \left[1 + \frac{\beta}{\alpha}(CI_j - CI_M)\right] \tag{13}$$

where CI_M is the mean climatic index, averaged on the studied watersheds, and CI_j is the climatic index value of the elementary area j, whereas β is a new fitting parameter, whose dimension depends on the specific climatic index adopted.

The structure of the proposed correlation implicitly simulates the idea underlying the SCS procedure (SCS 1972) that the watershed CN is derived from soil and land use data, and then it is separately adjusted according to AMC.

The regression procedure is undertaken by using the genetic algorithm (GA) implemented in GANetXL (Optimization Add-in for Microsoft Excel) (Savić *et al.* 2011); it searches for the values of the calibration parameters (α, β, and γ according to the specific model structure) that minimize the SSE, which is the objective function of the regression.

Goodness-of-fit statistics

Since the objective function (Equation (9)) is nonlinear, the most common measure for the goodness of fit, that is R^2, is inadequate (Cameron & Windmeijer 1997). In order to test the goodness of fit of the models, the root mean square error (RMSE) was adopted; RMSE can be expressed as follows:

$$\mathrm{RMSE} = \sqrt{\frac{SSE}{N-p}} \tag{14}$$

where p is the number of fitting parameters.

The Akaike information criterion, developed by Akaike (1974), can also be used to identify the appropriate model for the data; it can be obtained by calculating the mean square error of the model, as follows:

$$AIC = N \cdot \log(\mathrm{MSE}) + 2p \tag{15}$$

MSE is computed as follows:

$$\mathrm{MSE} = \frac{SSE}{N-p} \tag{16}$$

where all the parameters have been defined in the previous lines. As Equation (15) shows, AIC contains a penalty function increasing with the number of parameters; for this reason, it is particularly adequate to sort the best among different models, or among different expressions for the same model, but with an increasing number of parameters, as in the present paper. The best model is the one that has the minimum AIC value.

The raw values of AIC enable the choice of the best fitting model for the data but they are strongly dependent on the sample size. Conversely, the simple difference Δ_m of AIC values (Akaike 1978) allows assessment of the strength of evidence for each model m vs. the best one, namely the model with the minimum AIC value:

$$\Delta_m(AIC) = AIC_m - \min(AIC) \tag{17}$$

Typically, a Δ value within 1–2 suggests substantial evidence in favor of the model, which should be considered along with the best model, that is the one with the minimum AIC value.

Then the Akaike weights can be defined as follows (Burnham & Anderson 2002):

$$w_m(AIC) = \frac{\exp\left[-\frac{1}{2}\cdot\Delta_m(AIC)\right]}{\sum_{m=1}^{M}\left\{\exp\left[-\frac{1}{2}\cdot\Delta_m(AIC)\right]\right\}} \tag{18}$$

where w_m (AIC) is the weight for every model, Δ_m (AIC) is the relative AIC computed by applying Equation (17) for

each model, and M is the number of different models considered. Note that $\sum_{m=1}^{M} w_m$ is equal to 1.

Once the Akaike weights are known, one can define how much Model A better fits the data than Model B by simply putting into ratio their weights.

DISCUSSION

Histograms in Figure 3 show details about soil permeability within the investigated watersheds; although a prevalence of type B soils (moderate infiltration rates) exists, a significant presence of the other three soil types can be observed (Figure 3(a)). In Figure 3(b), where land use codes are replaced by the id numbers in Table 4, a broad predominance of 2.1.1 (id 11 – non-irrigated arable land) and 3.1.1 (id 21 – broad-leaved forest) can be observed, covering about 37 and 25% of the whole examined area, respectively. Nevertheless, even though a high percentage of area is covered by fairly permeable soil group and land uses, the two conditions do not necessarily occur simultaneously; as a result, as Figure 3(c) shows, 70% of the investigated area is characterized by rather small values of S, that suggests a medium–low permeability level.

In Figure 4, evaporation ratio ET/R is plotted against the Budyko Index ϕ for the 50 available watersheds symbolically indicated according to the region to which they belong (i.e., Calabria, Basilicata, Puglia, and Campania). As $\phi > 1$, that is for dry soils, available energy is a fraction of the amount required to evaporate the entire annual precipitation, so that the annual evapotranspiration approaches potential evaporation; as $\phi < 1$, that is for wet soils, annual evapotranspiration approaches annual precipitation, since the available energy exceeds the amount required to evaporate annual precipitation. The intersection point between the asymptotes marks a transition from energy-limited evapotranspiration (wet or humid watersheds) to a water-limited one (dry or arid watersheds). Figure 4 also confirms that Calabria is the wettest region in southern Italy, while Puglia is the most arid; indeed, their basins are plotted as the extreme points in the graph.

Figure 5(a) shows the relation between the observed flood runoff coefficients and the basin-averaged S values. Although huge variability can be observed, small S values (representative of rather impermeable surfaces) are associated with high φ_o, whereas high S values (representative of very permeable surfaces) are associated with small φ_o.

Minimizing SSE provides $\alpha = -0.017\ \mathrm{mm}^{-1}$ and $\gamma = 0.41$, with an SSE value equal to 0.9036. The rather high value of the square sum of errors, that is a rather high value of the unexplained variance, demonstrates that hydrogeological formations and land use are not the only factors affecting the runoff coefficient. This is evident in Figure 6, where the flood runoff coefficient values, represented as a function of S, are plotted in different shades according to their values of CI; as one would expect, great CI values (that is wet climate conditions) cause a decrease in the permeability of a specific soil, meant as a specific geology–land use combination, so that an increase in the runoff coefficient occurs. Conversely, small CI values (that is dry climate conditions) cause an increase in permeability, and a consequent decrease in the runoff coefficient.

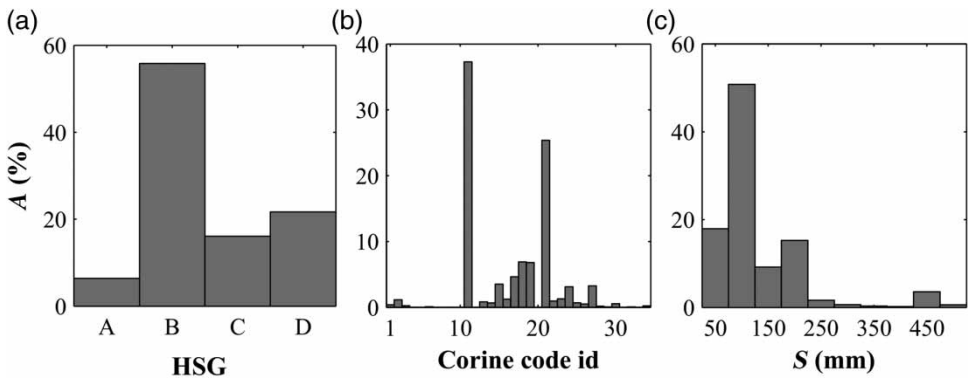

Figure 3 | Soil properties of investigated watersheds.

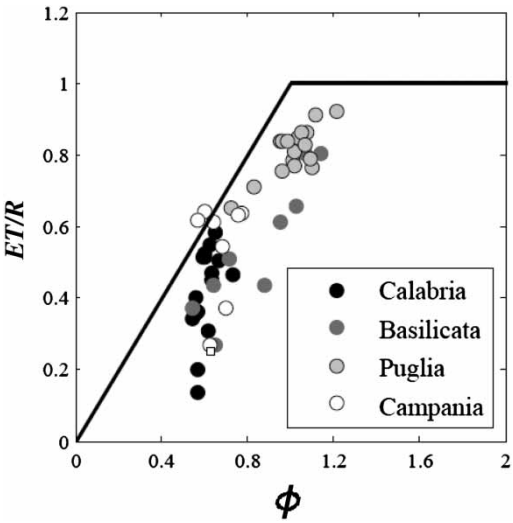

Figure 4 | Regional relation between Budyko Index and ratio of actual evapotranspiration to rainfall.

Figure 7(a) shows the results of the regression procedure when surface lithology, land use and climate controls, that is S and precipitation P, are considered. Minimizing the SSE provides $\alpha = -0.048\ \mathrm{mm}^{-1}$, $\beta = 3.33 \times 10^5\ \mathrm{mm}^{-2}$, and $\gamma = 2.82$; the improved relation has $SSE = 0.8129$. If Equation (13) is considered with $P = P_M$, that means assuming the Italian average climatic condition, the actual effect of geologic and land use controls can be seen, with $SSE = 1.0914$ (Figure 7(b)).

When the Budyko Index ϕ is considered as a climatic control, minimizing the SSE provides $\alpha = -0.02\ \mathrm{mm}^{-1}$, $\beta = 0.0084\ \mathrm{mm}^{-1}$, and $\gamma = 0.62$, with $SSE = 0.7671$; the observed and estimated runoff coefficients are shown in Figure 7(c). If Equation (13) is considered with $\phi = \phi_M$, that means assuming the Italian

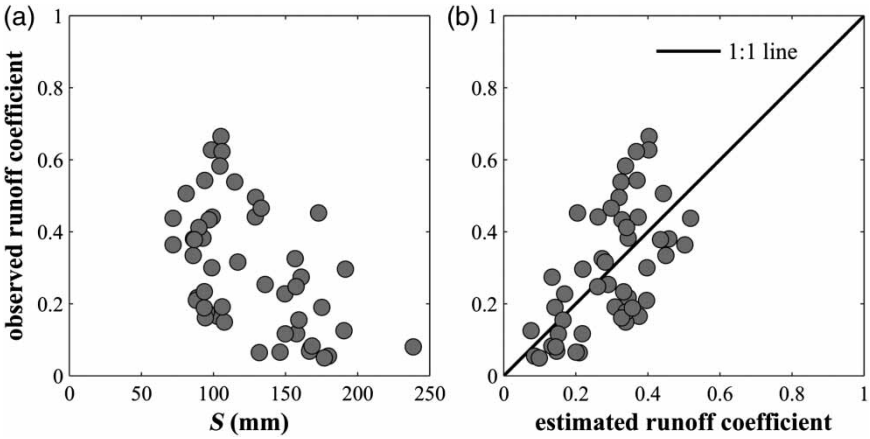

Figure 5 | Scatter of maximum potential retention S versus observed runoff coefficient φ (a); results of regression by considering the geologic control (b).

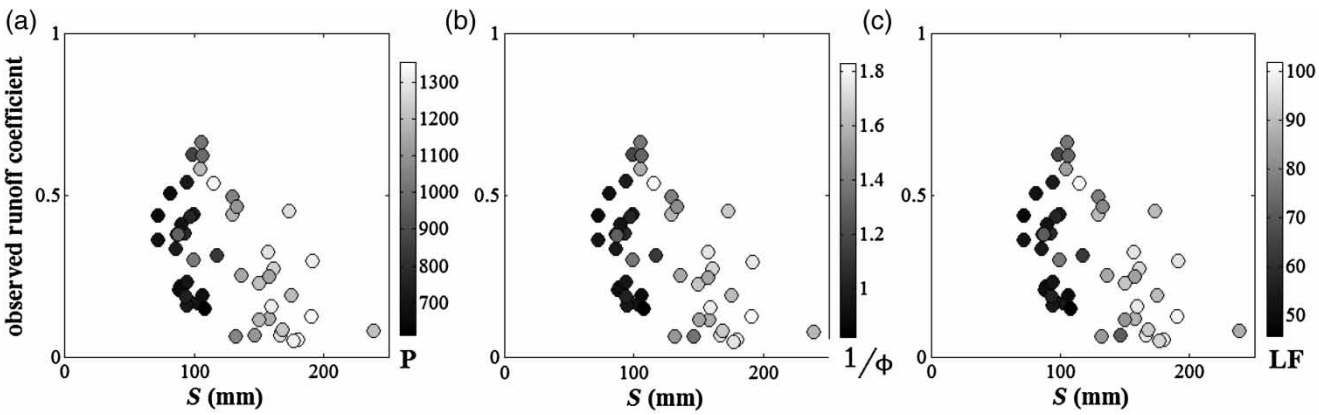

Figure 6 | Dependence of observed runoff coefficient on *CI*: mean annual precipitation P (a); reciprocal of Budyko Index $1/\phi$ (b); Lang Pluviofactor *LF* (c).

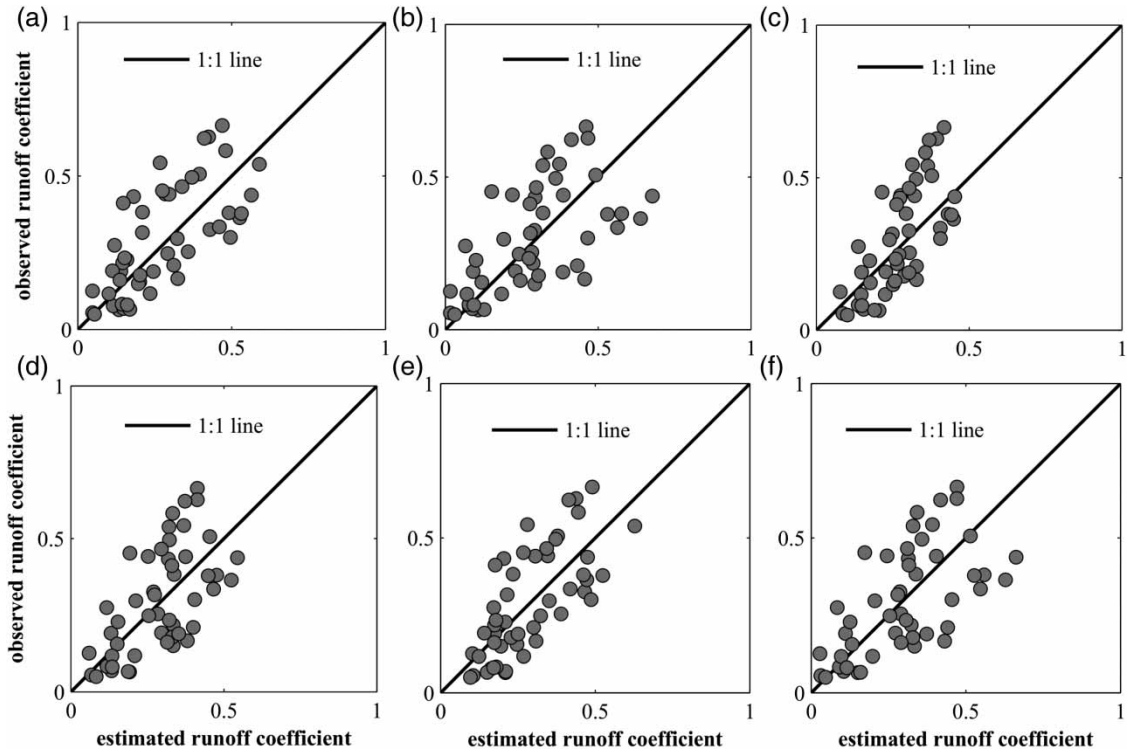

Figure 7 | Regression results by considering climate controls: mapped mean annual precipitation P (a) and a constant value P_M (b); mapped mean annual Budyko Index ϕ (c) and a constant value ϕ_M (d); mapped mean annual Lang Pluviofactor LF (e) and a constant value LF_M (f).

average climatic condition, the actual effect of geologic and land use controls can be seen, with $SSE = 0.9092$ (Figure 7(d)).

Finally, if Lang Pluviofactor LF is considered, the fitting procedure provides $\alpha = -0.032\ \mathrm{mm}^{-1}$, $\beta = 3.55 \times 10^{-4}\ \mathrm{mm}^{-2}\,^{\circ}\mathrm{C}$ and $\gamma = 1.6$, with $\mathrm{SSE} = 0.7492$; the observed and estimated flood runoff coefficients are shown in Figure 7(e). If Equation (13) is considered with $LF = LF_M$, that means assuming the Italian average climatic condition, the actual effect of geologic and land use controls can be seen, with $SSE = 1.0161$ (Figure 7(f)).

Table 5 shows a synthesis of the implemented regressions; comparing SSE values, the model including both the maximum potential retention and the Lang Pluviofactor, along with the Budyko Index in a slightly smaller measure, proves to give the best fit of experimental data. Table 6 gives details of the statistical parameters of the regression; the model including the Lang Pluviofactor has the minimum value of mean square error, RMSE and Akaike information criterion. By comparing the Akaike weights of every model to the best one, LF proves to be a 1.3 times more representative index than ϕ and 2.4 times more than P; furthermore, it proves to be 2.2 times more appropriate than the model considering only the soil effect.

The scattering of data in Figure 7 shows that a significant portion of variance in the flood runoff coefficients still remains unexplained; this is due to many causes, including an overall uncertainty in all the measured data, affecting the observed runoff coefficient values, and the possible existence of other influent variables that were not considered in the proposed model. Figure 8 plots the residuals r, namely the difference between observed and estimated flood runoff coefficients (accounting for S and LF), as a function of the watershed area, river length, mean river slope, time of concentration. A graphic analysis of residuals shows that none of these variables has a direct influence on the runoff coefficient; indeed, no particular trend can be observed in the residuals plot, with reference to any of the considered additional variables. Standardized residuals, defined in Equation (19), are provided in Figure 9, which

Table 5 | Parameters of the regression

Variables in the model	SSE	α (mm^{-1})	β	γ	CI_M
S	0.9036	-1.68×10^{-2}	–	4.06×10^{-1}	–
S, P	0.8129	-4.76×10^{-2}	3.33×10^{-5}	2.82	993.63
S, ϕ	0.7671	-1.96×10^{-2}	-8.43×10^{-3}	6.16×10^{-1}	0.7498
S, LF	0.7492	-3.17×10^{-2}	3.55×10^{-4}	1.60	73.94
S, $P=P_M$	1.0914	-0.047605	3.33×10^{-5}	2.815671	993.634
S, $\phi=\phi_M$	0.9092	-1.96×10^{-2}	-8.43×10^{-3}	6.16×10^{-1}	0.7498
S, $LF=LF_M$	1.0161	-3.17×10^{-2}	3.55×10^{-4}	1.60	73.94

Note: β dimensions are [mm^{-2}], [mm^{-1}], [mm^{-2}°C] when P, ϕ, LF are used as CI, respectively; CI_M dimensions are [mm], [adimensional], [mm °C^{-1}] when P, ϕ, LF are used as CI, respectively. See the text for description of the symbols.

Table 6 | Goodness of fit

Variables in the model	MSE	RMSE	AIC	$\Delta(AIC)$	$w(AIC)$	$w_{S,LF}(AIC)/w(AIC)$
S	0.01883	0.1372	– 82.2629	1.613	0.16963	2.241
S, P	0.0173	0.1315	– 82.1028	1.773	0.156584	2.427
S, ϕ	0.01632	0.1278	– 83.361	0.515	0.293727	1.294
S, LF	0.01594	0.1263	– 83.8763	0.000	0.380059	1.000

Note: β dimensions are [mm^{-2}], [mm^{-1}], [mm^{-2}°C] when P, ϕ, LF are used as CI, respectively; CI_M dimensions are [mm], [adimensional], [mm °C^{-1}] when P, ϕ, LF are used as CI, respectively. See the text for description of the symbols.

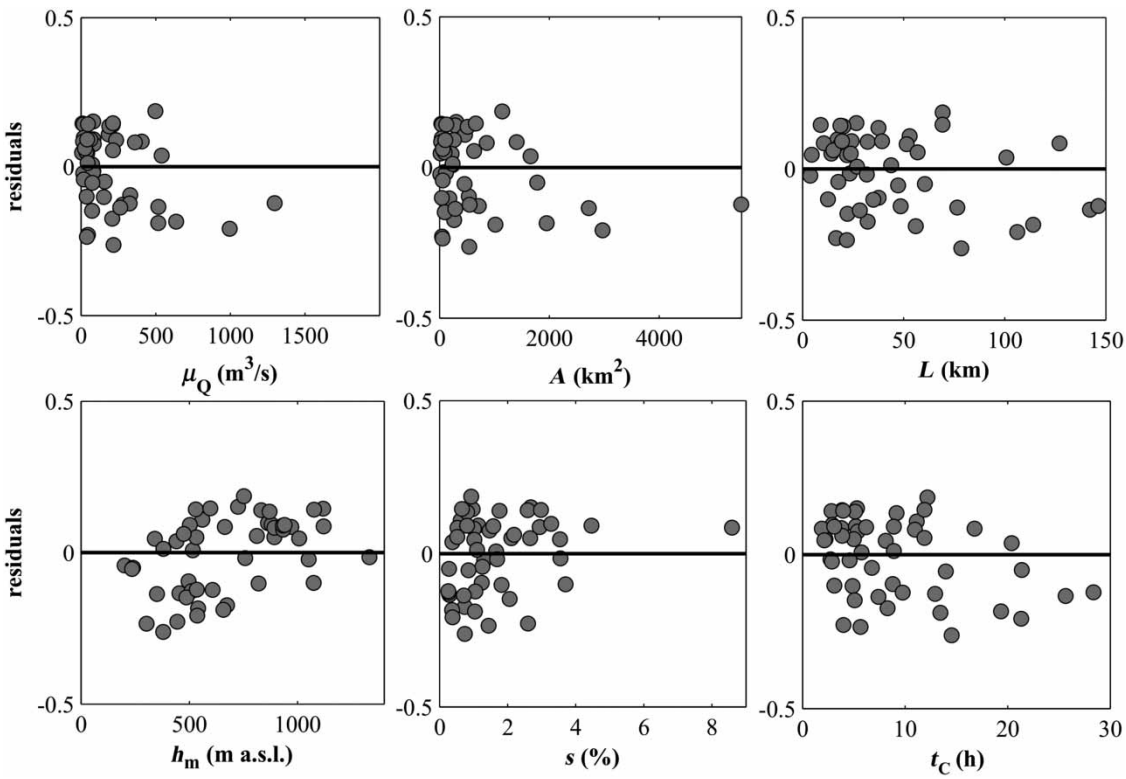

Figure 8 | Dependence of residuals r on some features of investigated watersheds.

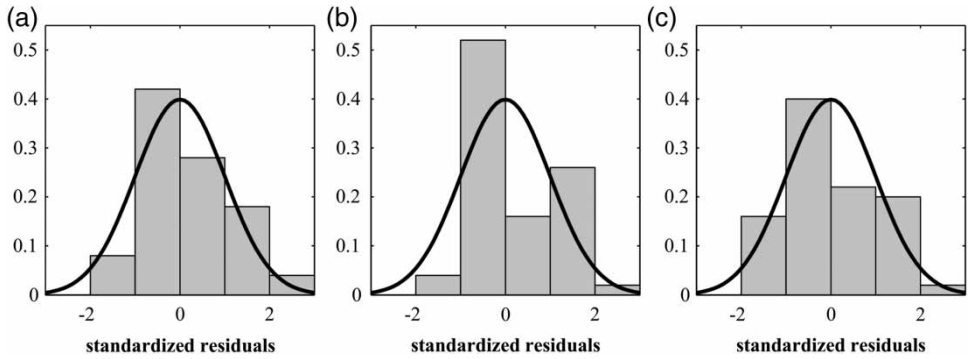

Figure 9 | Standardized residuals: S and P are considered in model (a); S and ϕ are considered in model (b); S and LF are considered in model (c).

confirms the hypothesis of a normal distribution for the residuals.

$$r_{st,i} = \frac{(\varphi_{o,i} - \varphi_{e,i}) \cdot N}{\sum_{i=1}^{N} (\varphi_{o,i} - \varphi_{e,i})^2} \tag{19}$$

where $r_{st,i}$ is the standardized residual for each watershed, and the other symbols have been defined previously.

CONCLUSIONS

In the present paper, an analysis was undertaken in order to investigate a possible dependence of the flood runoff coefficient on both soil and climate controls. The studied area includes 50 watersheds located within Southern Peninsular Italy, which can be considered a significant sample of the whole area highlighted in Figure 1, since they show a significant variability in both morphological and climatic features. Surface lithology and land use were quantified by adopting the SCS permeability classification, suitably applied to the considered soils by using a hydrogeological and a land use mapping; thus, each geology–land use combination is characterized by a certain value of maximum potential retention S. Different CI were defined, based on the available climatic data, namely mean annual precipitation and temperature; mean annual precipitation P, Budyko Index ϕ and Lang Pluviofactor LF were considered. A model accounting for both soil and climate controls was developed for the estimate of flood runoff coefficients, and results were compared to the observed values, which were derived from the application of the rational method within each gauged watershed. Results of the investigated correlations show that both soil and climate have a significant influence on the flood runoff coefficient; furthermore, according to the statistical results, the variable that best interprets climate proves to be the Lang Pluviofactor, closely followed by the Budyko Index. An explorative analysis was carried out in order to find other explicative variables, such as watershed area, river length, mean river slope, and time of concentration, but with no result. Figure 10 shows a map of φ achieved by graphically applying Equations (10)–(13) assuming $CI = LF$. The so computed runoff coefficient values enable the estimation of the mean annual maximum flood peak discharge in any ungauged watershed within Southern Peninsular Italy, by applying the rational method, once the

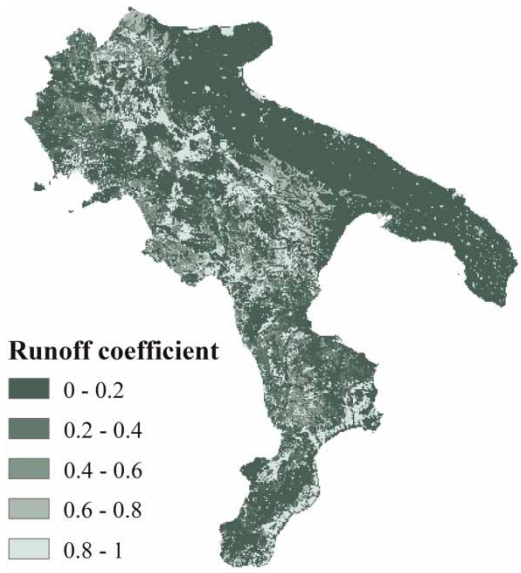

Figure 10 | Runoff coefficient map within Southern Peninsular Italy.

IDF curves and the areal reduction factor are known thanks to a regional analysis.

REFERENCES

Akaike, H. 1974 A new look at the statistical model identification. *IEEE T. Automat. Contr.* **19**, 716–723.

Akaike, H. 1978 On the likelihood of a time series model. *Statistician* **27**, 217–235.

Allocca, V., Celico, F., Celico, P., De Vita, P., Fabbrocino, S., Mattia, C., Monacelli, G., Musilli, I., Piscopo, V., Scalise, A. R., Summa, G. & Tranfaglia, G. 2007 *Note illustrative della carta idrogeologica dell'Italia Meridionale* (Hydrogeological Map of Southern Italy: illustrative notes). Istituto Poligrafico e Zecca dello Stato, Rome, Italy (in Italian).

Arora, V. K. 2002 The use of the aridity index to assess climate change effect on annual runoff. *J. Hydrol.* **265**, 164–177.

Beven, K. 2001 *Rainfall-Runoff Modelling: The Primer*. John Wiley & Sons, Chichester, UK.

Bossard, M., Feranec, J. & Otahel, J. 2000 CORINE land cover technical guide – Addendum 2000. European Environment Agency Technical report No. 40, Copenhagen, Denmark.

Brath, A., Castellarin, A., Franchini, M. & Galeati, G. 2001 Estimating the index flood using indirect methods. *Hydrol. Sci. J.* **46** (3), 399–418.

Budyko, M. I. 1974 *Climate and Life*. Academic Press, Orlando, FL.

Burnham, K. P. & Anderson, D. R. 2002 *Model Selection and Multimodel Inference: A Practical Information-theoretic Approach*. Springer-Verlag, New York.

Cameron, A. C. & Windmeijer, F. A. G. 1997 An R-squared measure of goodness of fit for some common nonlinear regression models. *J. Econ.* **77**, 329–342.

Cerdan, O., Le Bissonnais, Y., Govers, G., Leconte, V., Van Oost, K., Couturier, A., King, C. & Dubreuil, N. 2004 Scale effects on runoff from experimental plots to catchments in agricultural areas in Normandy. *J. Hydrol. Amsterdam* **299**, 4–14.

Claps, P., Copertino, V. A. & Fiorentino, M. 1994 Analisi regionale dei massimi annuali delle portate al colmo di piena. In: *Valutazione delle piene in Puglia* (*Flood evaluation in Puglia*) (V. A. Copertino & M. Fiorentino, eds). DIFA-University of Basilicata and CNR-GNDCI, Potenza, Italy (in Italian).

Cunnane, C. 1988 Methods and merits of regional flood frequency analysis. *J. Hydrol.* **100**, 269–290.

Dalrymple, T. 1960 Flood frequency analysis. Water Supply Paper 1543-A, US Geol. Survey, Reston, VA, USA.

Eagleson, P. S. 1972 Dynamics of flood frequency. *Water Resour. Res.* **8** (4), 878–898.

Giandotti, M. 1934 Previsione delle piene e delle magre dei corsi d'acqua (River flood and low-water discharge prevision). Memorie e studi idrografici, Pubbl. 2 del Servizio Idrografico Italiano, 8, 107 (in Italian).

Gottschalk, L. & Weingartner, R. 1998 Distribution of peak flow derived from a distribution of rainfall volume and runoff coefficient, and a unit hydrograph. *J. Hydrol. Amsterdam* **208**, 148–162.

Hargreaves, G. H. & Samni, Z. A. 1982 Estimation of potential evapotranspiration. *J. Irrigat. Drain. Div., Proceedings of the American Society of Civil Engineers* **108**, 223–230.

Hosking, J. R. M. & Wallis, J. R. 1997 *Regional Frequency Analysis: An Approach Based on L-Moments*. Cambridge University Press, Cambridge, UK.

Iacobellis, V. & Fiorentino, M. 2000 Derived distribution of floods based on the concept of partial area coverage with a climatic appeal. *Water Resour. Res.* **36**, 469–482.

IH 1999 *Flood Estimation Handbook*. Institute of Hydrology, Wallingford, UK.

Kjeldsen, T. R. & Jones, D. A. 2010 Predicting the index flood in ungauged UK catchments: On the link between data-transfer and spatial model error structure. *J. Hydrol.* **387**, 1–9.

Koutsoyiannis, D. & Manetas, A. 1998 A mathematical framework for studying rainfall intensity duration-frequency relationships. *J. Hydrol.* **206** (1–2), 118–135.

Lang, R. 1915 Versuch einer exakten Klassifikation der Boden in klimatischer und geologischer Hinsicht (An attempt at a climatic and geological classification of soils). *International Mittelingen Bodenkunde* **5**, 312–346 (in German).

Mancini, M. & Rosso, R. 1989 *Using GIS to assess spatial variability of SCS Curve Number at the basin scale*. New Directions for Surface Water Modeling, IAHS Publication No 181, IAHS Press, Wallingford, UK, pp. 435–444.

Merz, R. & Blöschl, G. 2009 A regional analysis of event runoff coefficients with respect to climate and catchment characteristics in Austria. *Water Resour. Res.* **45**, W01405.

Merz, R., Blöschl, G. & Parajka, J. 2006 Spatio-temporal variability of event runoff coefficients. *J. Hydrol.* **331**, 591–604.

Miliani, F., Ravazzani, G. & Mancini, M. 2011 Adaptation of precipitation index for the estimation of antecedent moisture condition in large mountainous basins. *J. Hydrol. Eng.* **16** (3), 218–227.

Mishra, S. K., Kumar, S. R. & Singh, V. P. 1999 Calibration and validation of a general infiltration model. *Hydrol. Process.* **13** (11), 1691–1718.

Moisello, U. 1999 *Idrologia Tecnica* (Technical Hydrology). La Goliardica Pavese, Pavia, Italy (in Italian).

Monteith, J. L. 1965 Evaporation and environment. In: *Symposium of the Society for Experimental Biology, The State and Movement of Water in Living Organisms* (G. E. Fogg, ed.). Academic Press, NY, Vol. 19, pp. 205–234.

Mulvaney, T. J. 1851 On the use of self-registering rain and flood gauges in making observations of the relations of rainfall and of flood discharges in a given catchment. *Proc. Inst. Civil Eng. Ireland* **4**, 18–31.

Naef, F. 1993 Der Abflusskoeffizient: einfach und praktisch? (The runoff coefficient: easy and convenient?) In: Aktuelle Aspekte

in der Hydrologie (Present issues of Hydrology) Zürcher Geographische Schriften, Heft 53, Verlag Geographisches Institut ETH Zürich, pp. 193–199 (in German).

Ol'dekop, E. M. 1911 On evaporation from the surface of river basins. *Trans. Met. Obs. Iurevskogo, Univ. Tartu* **4** (in Russian).

Penman, H. L. 1948 Natural evaporation from open water, bare soil, and grass. *Proc. Roy. Soc. London* **A193**, 120–146.

Penta, A., Rasulo, G. & Rossi, F. 1972 Criteri di similitudine idrologica per l'analisi dei massimi annuali di pioggia (Hydrological similitude criteria for the analysis of annual maximum flood peak discharges). Proc. CIGR Conf., Florence, Italy (in Italian).

Pike, J. G. 1964 The estimation of annual runoff from meteorological data in a tropical climate. *J. Hydrol.* **2**, 116–123.

Preti, E., Forzieri, G. & Chirico, G. B. 2011 Forest cover influence on regional flood frequency assessment in Mediterranean catchments. *Hydrol. Earth Syst. Sci.* **15**, 3077–3090.

Priestley, C. H. B. & Taylor, R. J. 1972 On the assessment of surface heat flux and evaporation using large-scale parameters. *Mon. Wea. Rev.* **100**, 81–92.

Ranzi, R., Bochicchio, M. & Bacchi, B. 2002 Effects on floods of recent afforestation and urbanisation in the Mella River (Italian Alps). *Hydrol. Earth Syst. Sci.* **6** (2), 239–253.

Rasulo, G., Del Giudice, G. & Calcaterra, D. 2009 Flood index assessment. Relation between runoff coefficient and the SCS Soil-Cover Complexes. *L'Acqua* **2**, 37–44 (in Italian).

Riggs, H. C. 1973 *Regional analysis streamflow characteristics*. US Geological Survey Water Resources Invest. Tech., Book 4.

Rossi, F. & Villani, P. 1994 *Valutazione delle Piene in Campania* (Flood evaluation in Campania). CNR-GNDCI, Publ. No. 1472, Grafica Matelliana & C., Cava de' Tirreni (SA), Italy (in Italian).

Rossi, F., Fiorentino, M. & Versace, P. 1984 Two-component extreme value distribution for flood-frequency analysis. *Water Resour. Res.* **20** (7), 847–856.

Sahu, R. K., Mishra, S. K. & Eldho, T. I. 2010 An improved AMC-coupled runoff curve number model. *Hydrol. Process.* **24** (20), 2834–2839.

Savić, D. A., Bicik, J. & Morley, M. S. 2011 A DSS generator for multiobjective optimisation of spreadsheet-based models. *Environ. Model. Softw.* **26** (5), 551–561.

Scherrer, S., Naef, F., Faeh, O. & Cordery, I. 2007 Formation of runoff at the hillslope scale during intense precipitation. *Hydrol. Earth Syst. Sci.* **11**, 907–922.

Schreiber, P. 1904 Ueber die Beziehungen zwischen dem Niederschlag und der Wasseruhrung der Flusse in Mitteleuropa. *Meteorol. Z.* **21**, 441–452 (in German).

SIMN 1921–1994 *Annali idrologici* (Hydrologic Yearbooks). Servizio Idrografico e Mareografico Nazionale, Naples, Bari and Catanzaro Departments, Istituto Poligrafico dello Stato, Roma, Italy (in Italian).

Sivapalan, M., Blöschl, G., Merz, R. & Gutknecht, D. 2005 Linking flood frequency to long-term water balance: incorporating effects of seasonality. *Water Resour. Res.* **41** (6), W06012.

Smith, A. A. & Lee, K. B. 1984 The rational method revisited. *Can. J. Civ. Eng.* **11**, 854–862.

Soil Conservation Service (SCS) 1972 Section 4*: Hydrology*. US National Engineering Handbook, US Department of Agriculture, Washington, DC.

Thornthwaite, C. W. 1948 An approach toward a rational classification of climate. *Am. Geogr. Rev.* **38** (1), 55–94.

Turazza, D. 1880 *Trattato di idraulica pratica* (Practical Hydraulics Essay). F. Sacchetto, Padova (in Italian).

Turc, L. 1954 Le bilan d'eau des sols. Relation entre la précipitation, l'évaporation et l'écoulement (Soil water balance: relation among precipitation, evaporation and runoff). *Ann. Agron.* **5**, 491–569 (in French).

van Dijk, A. I. J. M. 2010 Selection of an appropriately simple storm runoff model. *Hydrol. Earth Syst. Sci.* **14**, 447–458.

Versace, P., Ferrari, E., Fiorentino, M., Gabriele, S. & Rossi, F. 1989 *Valutazione delle Piene in Calabria* (Flood evaluation in Calabria). CNR-IRPI and GNDCI, Geodata, Cosenza, Italy (in Italian).

Viglione, A., Merz, R. & Blöschl, G. 2009 On the role of the runoff coefficient in the mapping of rainfall to flood return periods. *Hydrol. Earth Syst. Sci.* **13**, 577–593.

Wainwright, J. & Parson, A. J. 2002 The effect of temporal variations in rainfall on scale dependency in runoff coefficients. *Water Resour. Res.* **38** (12), 1271–1281.

Wang, X., Liu, T. & Yang, W. 2012 Development of a robust runoff-prediction model by fusing the Rational Equation and a modified SCS-CN method. *Hydrolog. Sci. J.* **57** (6), 1118–1140.

First received 21 December 2012; accepted in revised form 14 June 2013. Available online 18 July 2013